FAST Observations of Electromagnetic Stresses Applied to the Polar Ionosphere

R. J. Strangeway

Institute of Geophysics and Planetary Physics, University of California at Los Angeles, Los Angeles, California

R. C. Elphic

Los Alamos National Laboratory, Los Alamos, New Mexico

W. J. Peria and C. W. Carlson

Space Sciences Laboratory, University of California at Berkeley, Berkeley, California

The Fast Auroral Snapshot Explorer (FAST), with its 83 inclination orbit and 4000 km apogee, is ideally suited for investigation of the high latitude perturbations to the geomagnetic field. These data can be used to determine field-aligned currents, but here we emphasize the perturbations themselves, rather than their spatial gradient. This allows us to more readily visualize the forces applied to the ionosphere by the magnetosphere (and vice-versa). Our basic framework for interpreting the magnetic field perturbations is one in which flows in the magnetosphere and at the magnetopause apply stresses to the ionosphere where the imposed flows must overcome the collisional drag. Thus field-aligned currents flow in response to a requirement for an ionospheric $\mathbf{J} \times \mathbf{B}$ force to overcome the drag. We will interpret two intervals of polar data acquired by FAST in this framework, showing how the overall structure of the field perturbations can be understood in terms of applied stresses. We discuss briefly one implication of this approach, that the ionosphere may be important in braking substorm-related flow bursts.

1. INTRODUCTION

It has long been known that Field-Aligned Currents (FACs) flow into and out of the polar ionosphere. The earliest observations of low altitude field-aligned currents were by *Zmuda et al.* [1966], who reported transverse magnetic disturbances at 1100 km altitude, as measured by satellite 1963-38C. Although Zmuda et al. originally attributed the disturbances to hydromagnetic waves, *Cummings and Dessler* [1967] presented a convincing argument that the disturbances could best be attributed to field-aligned currents. Indeed in later studies using Triad magnetometer data, *Armstrong and Zmuda* [1973] and *Zmuda and Armstrong* [1974a,b] discussed the magnetic perturbations almost entirely in terms of field-aligned currents.

Zmuda and Armstrong [1974b] also organized their observations of FACs, showing a characteristic and now familiar distribution of currents, where the currents lie in two concentric circles roughly collocated with the auroral oval. *Iijima and Potemra* [1976] named these currents Region 1 and Region 2. Region 1 currents flow into the ionosphere on the dawnside of the high latitude auroral oval, and out on the dusk side. Region 2 currents flow in the opposite sense at lower latitudes. *Iijima and Potemra* [1976] and *Sugiura and Potemra* [1976] both pointed out that there need not be local closure of the field-aligned currents. *Iijima and Potemra* [1976] noted that Region 1 currents tended to be larger than region 2 currents, while *Sugiura and Potemra* [1976] noted a "steplike level shift."

The presence of a stepwise change in the transverse field on crossing the auroral oval can be interpreted in terms of electromagnetic stress applied to the polar ionosphere, presumably by some form of high altitude generator, either at the magnetopause or in the equatorial magnetosphere. Viewing transverse perturbations of the magnetic field in terms of stress, rather than in terms of field-aligned cur-
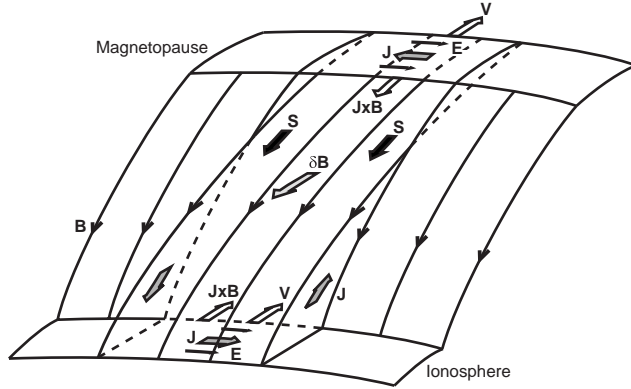
Figure 1. Cartoon showing the relationship between the applied flows at the magnetopause and the resultant stresses and flows at the ionosphere. Although drawn for the case of magnetopause flows, the sketch can be applied to magnetospheric flows. In the latter case the field lines should be traced to the equatorial region, and the high altitude flow would be earthward.

rents, is a theme also taken up by *Elphic et al.* [this issue], and reflects the arguments set forth by *Parker* [1996]. Note, however, that the use of the "B, v paradigm" does not preclude consideration of "E, j", but rather it lets us use a framework for determining the currents and electric fields that exist as a consequence of the applied flows and stresses.

In the next section we will present a simple cartoon relating high altitude magnetospheric and magnetopause drivers to the ionospheric response. We will then present examples of magnetometer data from the Fast Auroral Snapshot (FAST) explorer, emphasizing the interpretation of the observed signatures in terms of applied stress. In the concluding section we will summarize our analysis, and also address some comments to the role of ionospheric drag as a mechanism for flow braking within the inner magnetosphere.

2. IONOSPHERIC RESPONSE TO APPLIED STRESS

Figure 1 presents a simple cartoon of the ionospheric response to a driver at high altitudes. In this case we are assuming that the driver is a region of enhanced flux transport at the magnetopause. Such enhanced transport could arise from localized reconnection. Near the reconnection site the magnetopause flow is accelerated by the $\mathbf{J} \times \mathbf{B}$ "slingshot", but further downstream the reconnected flux tubes which thread the magnetopause will be transported by the magnetosheath flow, and it is this enhanced flux transport which ultimately drives field-aligned currents.

We note that this picture could as easily apply to processes such as substorms, where flow bursts, which are also regions of enhanced flux transport, appear to drive field-aligned currents into the ionosphere [*Shiokawa et al.* 1998]. In this case the high altitude region in Figure 1 should be mapped to the equator, and the flow would be directed earthwards.

At the high altitude end of the field lines in Figure 1 a region of enhanced tailward flow (**V**) carries field lines downstream (into the page in the figure perspective). The ambient magnetic field (**B**) has a normal component through the top surface (the magnetopause), which results in a convection electric field ($\mathbf{E} = -\mathbf{V} \times \mathbf{B}$). Furthermore, the downstream flow acts to stretch the field lines, giving a $\delta \mathbf{B}$ in the upstream direction. The current (**J**) associated with this $\delta \mathbf{B}$ opposes the convection **E**, and the magnetopause current layer is a generator, i.e., a source of electromagnetic energy. In addition, the $\mathbf{J} \times \mathbf{B}$ force in the layer opposes the flow. This is the drag on the flow due to the increased tension in the stretched field lines.

At this stage, we have not yet stated where the drag on the flow comes from. Increasing the tension along the field requires that at some location the convection of the field lines is retarded. In Figure 1 this is the ionosphere. For the ionosphere to act as a drag on the magnetopause flow there must be communication between the two regions. This communication can be thought to occur via either Poynting flux ($\mathbf{S} = \mathbf{E} \times \delta \mathbf{B} / \mu_0$) or the field-aligned currents that current continuity requires at the edges of the high flow region.

At the ionospheric end of the field lines the field-aligned currents close via a horizontal current. The resultant ionospheric $\mathbf{J} \times \mathbf{B}$ force will accelerate the ionospheric plasma, and we can consider the field lines to be pulling the plasma in the direction of the magnetopause flow. This motion will be retarded by the collisional drag of the ionosphere, as ionospheric ions are forced to move through the neutral atmosphere. For collisions to act as a drag, the flow must of course be in the same direction as the $\mathbf{J} \times \mathbf{B}$ force. Thus the motional electric field is in the same direction as **J** and the ionosphere is a load with $\mathbf{J} \cdot \mathbf{E} > 0$.

Before considering the further ramifications of Figure 1, we should point out that this viewpoint is not particularly new. Indeed, *Coroniti and Kennel* [1973] used this methodology to discuss the role of ionospheric conductivity in controlling the rate of dayside magnetopause erosion. Similarly, *Cowley* [1981] discussed the effects of interplanetary magnetic field (IMF) B_y on polar cap flows and field-aligned currents in terms of applied stresses. More recently, *Wright* [1996] used this framework to discuss the transfer of energy and momentum from the magnetosheath, but he also included the effects of finite Alfvén velocity. We have ignored this here, but is clearly important in establishing an equilibrium between the ionosphere and the

magnetospheric and magnetopause drivers. Thus Figure 1 should be viewed as a framework for discussing the coupling between the ionosphere and the magnetosphere, and indeed we might expect many auroral and polar cap phenomena to be the signature of the negotiation that occurs as ionosphere and magnetosphere attempt to come to equilibrium.

Bearing in mind these limitations, we can nevertheless derive some useful scaling laws. First, mapping of the convection electric field requires

$$V_I B_0 L_I = f V_m B_n L_m \qquad (1)$$

where V_I is the ionospheric flow velocity, B_0 is the vertical ionospheric magnetic field, L_I is the ionospheric transverse scale-length (in the direction of the horizontal current), V_m is the magnetopause flow velocity, B_n is the normal component of the magnetic field, and L_m is the magnetopause transverse scale-length. The factor f takes into account the possibility of imperfect mapping of the electric field, with $0 \le f \le 1$. When $f = 1$ there is perfect mapping of the magnetopause convection electric field to the ionosphere. When $f \ne 1$ a parallel electric field is present which allows the ionosphere to decouple from the magnetosphere, and the ionosphere slips with respect to the magnetosphere. The transverse scale-lengths in (1) are largely set by field line mapping.

Current continuity requires

$$J_I/B_0 L_I = J_m/B_n L_m \qquad (2)$$

where J_I and J_m are current intensities.

For a current sheet, the magnetic field perturbation is given by $\delta B = \mu_0 J$ and

$$\delta B_I/B_0 L_I = \delta B_m/B_n L_m \qquad (3)$$

Combining (1) and (3) we find

$$E_I \delta B_I/B_0 = f E_m \delta B_m/B_n \qquad (4)$$

where E_I and E_m are the convection electric fields. Equation (4) states that the Poynting flux into the ionosphere equals that fraction of the Poynting flux from the magnetosphere that is not dissipated by parallel electric fields, with the ratio B_n/B_0 taking into account the change in flux tube area.

Last,

$$J_I = \Sigma_p V_I B_0 \qquad (5)$$

where Σ_p is the height-integrated Pedersen conductivity.

It should be noted that equations (1) and (5) both assume that $E_I = V_I B_0$. This implicitly assumes that although the ions do collide with neutrals, $v_{in} << \Omega_i$, where v_{in} is the ion-neutral collision frequency and Ω_i is the ion gyrofrequency. In this case the ions and electrons move with nearly identical bulk velocities, with the difference in their velocities giving the current.

When $v_{in} << \Omega_i$ the strong equivalence between drag and conductivity is readily apparent. In steady state the force law shows that

$$nm_i V_I v_{in} = j_I B_0 \qquad (6)$$

where n is the density, m_i is the ion mass, and j_I is the current density. Equation (6) is simply a statement that the momentum lost by the ions through collisions with neutrals is balanced by the $\mathbf{j} \times \mathbf{B}$ force. In making this statement we have implicitly assumed that V_I is the velocity of the ions with respect to the neutral gas, and further that the neutrals are a drag on the ion flow. This need not always be the case. For example, *Kelley* [1989], in his Chapter 7, discusses acceleration of neutrals by the $\mathbf{j} \times \mathbf{B}$ force. He shows that on occasion the neutrals can flow at the same velocity as the ions, under conditions of extremely steady convection lasting for several hours. *Deng et al.* [1991] have also examined the flywheel effect, where the neutrals can drive convection in the polar cap, although the magnetosphere-imposed convection is necessarily weak for this to occur.

Notwithstanding the ability of the neutrals to sometimes drive ionospheric flows, equation (6) points out that it is the ionospheric drag which determines the size of the current: the larger the drag force the larger the perpendicular current. This then leads to the equivalence between drag and conductivity. On replacing V_I with E_I/B_0, which assumes we can neglect the Hall term in the Ohm's law, we find

$$nm_i E_I v_{in}/B_0^2 = j_I \qquad (7)$$

Therefore

$$\sigma_p = ne^2 v_{in}/m_i \Omega_i^2 \qquad (8)$$

where σ_p is the Pedersen conductivity. Equation (8) gives the standard form of σ_p for $v_{in} << \Omega_i$.

We can combine equations (1), (3), and (5) to derive some useful scaling laws that relate ionospheric and magnetospheric parameters. From (1) and (5), since $\delta B_I = \mu_0 J_I$,

$$\delta B_I = f\left(\frac{L_m}{L_I}\right)\mu_0 \Sigma_p V_m B_n \qquad (9)$$

while from (3) and (5)

$$V_{\mathrm{I}} = \left(\frac{L_{\mathrm{I}}}{L_{\mathrm{M}}}\right)\frac{1}{\mu_0\Sigma_{\mathrm{p}}}\frac{\delta B_{\mathrm{m}}}{B_{\mathrm{n}}} \qquad (10)$$

and from all three

$$\delta B_{\mathrm{m}} = f\left(\frac{L_{\mathrm{m}}}{L_{\mathrm{I}}}\right)^2\left(\frac{B_{\mathrm{n}}}{B_0}\right)\mu_0\Sigma_{\mathrm{p}}V_{\mathrm{m}}B_{\mathrm{n}} \qquad (11)$$

Equation (9) states that the stress applied to the ionosphere increases for increasing ionospheric conductivity, but decreases if a parallel electric field is present ($f < 1$). Equation (10) states that for a given magnetic shear at the magnetopause, increasing the conductivity reduces the convection velocity in the ionosphere. Both of these statements are another way of saying that a highly conducting ionosphere acts as a drag on the higher altitude flows, and the forces required to move the ionosphere against this drag are larger.

Equation (11) relates the magnetopause stress to the magnetopause flow. Again, higher ionospheric conductivity results in higher stress. The stress is reduced if parallel electric fields are present.

Before discussing the consequences of these scaling laws it is worthwhile to determine if they provide reasonable estimates for the fields and flows. We shall assume that the flow velocity at the magnetopause (V_{m}) is 100 km/s, the normal component of the magnetic field (B_{n}) is 5 nT, and $\Sigma_{\mathrm{p}} = 10$ S. For the purposes of estimating transverse scale lengths we will assume $L_{\mathrm{m}}/L_{\mathrm{I}} \approx (B_0/B_{\mathrm{n}})^{1/2}$, and $B_0 = 50{,}000$ nT, i.e., $L_{\mathrm{m}}/L_{\mathrm{I}} = 100$. From (9), assuming no slippage, $\delta B_{\mathrm{I}} = 630$ nT. From (11), $\delta B_{\mathrm{m}} = 6.3$ nT, while from (10), $V_{\mathrm{I}} = 1$ km/s. That $V_{\mathrm{m}}/V_{\mathrm{I}} = \delta B_{\mathrm{I}}/\delta B_{\mathrm{m}} = L_{\mathrm{m}}/L_{\mathrm{I}}$ should not be surprising, this is simply a consequence of the mapping, but it is noteworthy that the inferred magnetic field perturbations are reasonable.

The scaling laws also show why the magnetosphere is usually thought to drive ionospheric convection, at least at higher latitudes. In their study *Deng et al.* [1991] found flywheel-driven currents of the order 0.04 µA/m². Although it is possible that the current densities were low because of the smearing inherent in the model they used, even assuming a current sheet of 10 width in latitude, we only obtain a current intensity of the order 40 mA/m. This gives $\delta B_{\mathrm{I}} \approx 50$ nT, an order of magnitude less than the estimate given above.

The scaling laws may shed some light on the observation of *Newell et al.* [1996] that auroral electron acceleration events occur mainly when the ionosphere is in darkness. For the dark ionosphere Σ_{p} is controlled largely by electron precipitation. Assuming a magnetospheric velocity shear, then the increased conductivity associated with the precipitating electrons carrying the upward current will require an increased current in the ionosphere. The current demand can be reduced by increasing the amount of slippage (decreasing f). At the same time, decreasing f, which requires a parallel electric field, will result in an increase in current density, and hence total current, as given by the Knight relation [*Knight*, 1973]. On the other hand, the sunlit ionosphere has a high conductivity and it might be expected that currents would preferentially flow to the sunlit hemisphere, rather than the dark ionosphere. For the sunlit ionosphere, however, the relatively uniform conductivity could allow an increase in field-aligned current intensity through a widening of the shear layer without increasing the field-aligned current density. Because the ionospheric currents in the dark ionosphere mainly flow in a high conductivity channel, perhaps the shear layer cannot increase in width in this case, and parallel electric fields are required. Thus, while the current may preferentially flow into the sunlit ionosphere, i.e., the field-aligned current *intensity* may be larger in the sunlit hemisphere, the field-aligned current *density* is likely to be larger in the dark hemisphere.

3. STRESSES IN THE POLAR CAP

As an example of the signatures observed in the polar cap we have analyzed FAST magnetometer data acquired on November 24th, 1996. This interval has been chosen by the Geospace Environment Modeling (GEM) community for an intense analysis and modeling effort. L. R. Lyons et al. ["Timing of Substorm Signatures During November 24, 1996 Geospace Environment Modeling Event", manuscript in preparation, 1999] describe the interval in greater detail, where two closely spaced substorm onsets occurred around 22:30 UT, following an extended interval of southward IMF. WIND data are shown in Figure 2. The data have been lagged by 15 minutes, which is an approximate lagtime for the prevailing solar wind conditions. The solid bars under the B_{z} trace indicate those time intervals for which FAST data were acquired in the northern polar cap and auroral zone. The corresponding FAST data are shown in Plate 1.
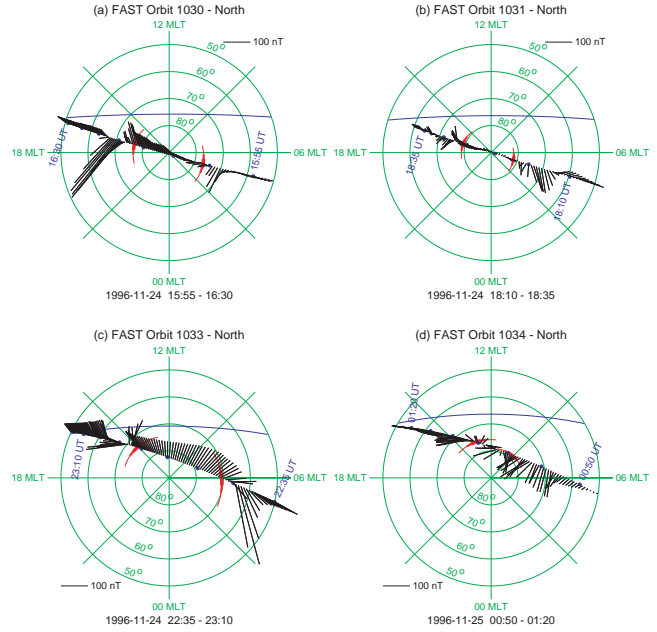
In Plate 1 the data are plotted using a polar projection. In this projection we initially cast the spacecraft position and magnetic field perturbations into SM coordinates. The spacecraft radius vector then defines a magnetic meridian perpendicular to the SM equator, and the transverse deviations with respect to the model field (IGRF 95 plus secular variation) are used to derive the magnitude and angle of the projected field perturbation. In this projection a vector that points away from the origin lies within the magnetic meridian plane and points to lower latitude. At high latitudes, where the ambient magnetic field is nearly vertical, there is no ambiguity. For more equatorial latitudes the projected field can appear to point in the opposite direction
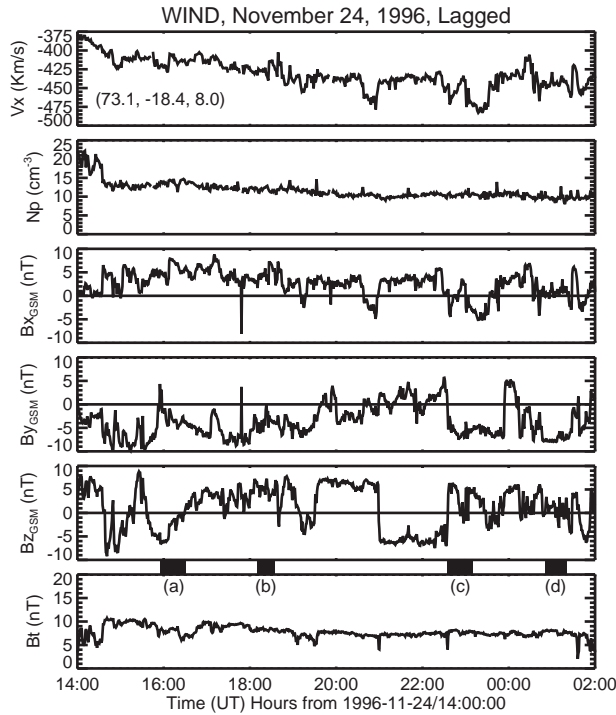
Figure 2. Solar wind data from the WIND spacecraft. The data have been lagged by 15 minutes, corresponding to nominal solar wind conditions. The top panel shows the x-component of the solar wind velocity. The position of the WIND spacecraft in GSE is given in parentheses in this panel. The next panel shows solar wind density. The bottom four panels show magnetic field data in GSM.

Plate 1. Polar projection of the magnetic field perturbations observed at FAST for the intervals indicated as solid bars in Figure 2. The data are plotted as a function of invariant latitude and magnetic local time along the spacecraft trajectory. The terminator is shown in blue, and the polar cap boundary, inferred from keV ion observations, is marked in red.

to the observed field, but this is simply a matter of mapping the perturbation vector along the ambient magnetic field. We should emphasize that we have not mapped the magnitude of the field perturbation to the ionosphere. This mapping will typically increase the magnitude of the perturbation by a factor of two for data acquired near FAST apogee. Last, although the magnetometer data are acquired at a high rate by FAST, we have averaged the data to 20-s samples, for ease of visibility.

In each panel approximately 40 minutes of data are shown. For these passes the spacecraft altitude is increasing with time, starting around 1000 km at the beginning of each pass, and approaching apogee (~4000 km) at the end of each pass. The spacecraft orbit is near the dawn-dusk meridian. In addition to the magnetic field perturbations, shown in black, we also mark the terminator with a blue line. The red arc segments mark the polar cap boundary. For the data in Plate 1 we have taken a sharp decreases in the flux of keV ions observed on FAST to determine the
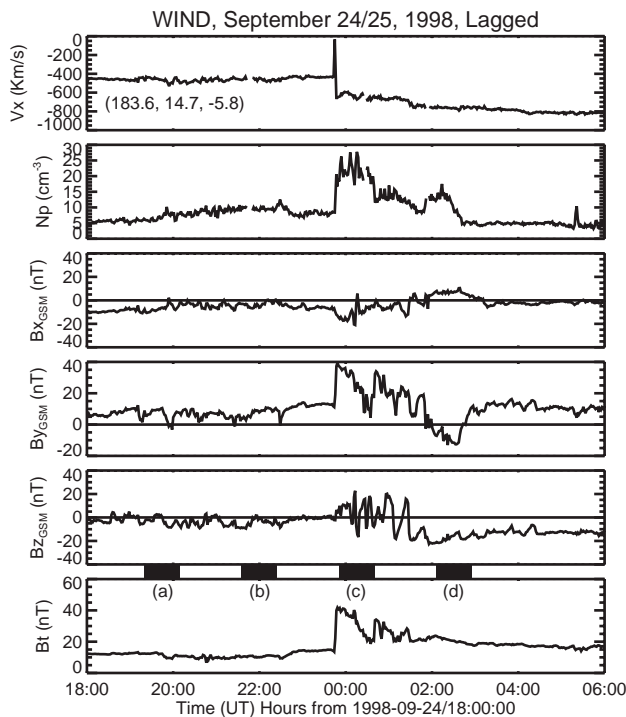
polar cap boundary (electron data were unavailable for these intervals).

In Plate 1a we see large deflections of the magnetic field in the pre-dusk auroral oval. This corresponds to an interval of southward IMF, and we expect convection to be strong at this time. The deflections in the field are consistent with the standard Region-1, -2 current system, and there is some indication that the polar cap field lines are being pulled tailward. In interpreting northern hemisphere data, it should be remembered that a sunward perturbation of the field corresponds to the field line being pulled tailward, and the ionospheric flows should be in the opposite direction to the field perturbation. For Plate 1b the IMF has been northward for quite some time, and the polar cap is small and quiet, with very little forcing by the IMF. The auroral-zone currents are weak. This interval also demonstrates that the magnetometer calibration and spacecraft attitude are well determined, since the residual fields are very small. The next panel, Plate 1c, shows the field perturbations after an extended interval of southward IMF. As noted by Lyons et al., two substorm onsets occurred near 22:30 UT. Using the framework discussed in the previous section, we would say that there is strong forcing of the
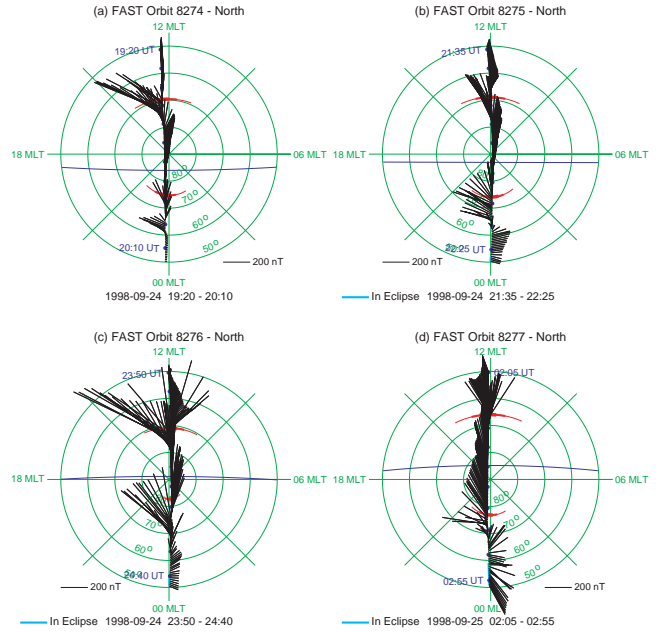
polar cap at this time. Last, Plate 1d shows the magnetic field perturbations after an extended interval of northward IMF. For this pass, FAST only briefly entered the polar cap, and there is some indication that the spacecraft is encountering cusp currents. Indeed the ion data show evidence of magnetosheath plasma entry, and these cusp ions make determination of the polar cap boundary somewhat difficult.

4. STRESSES IN THE CUSP

Figure 3 and Plate 2 show data for an interval studied by *Moore et al.* [1999], where intense ionospheric outflows are observed after the passage of an interplanetary shock and a coronal mass ejection (CME). Figure 3 shows WIND data. The interplanetary shock occurs at a lagged time of 23:45 UT, followed by the CME, marked by the roughly linear trend in IMF B_y from 00:35 to 02:35 UT (lagged). The data have been lagged such that the shock occurs at the same time as the Sudden Impulse within the magnetosphere. For most of the interval prior to the shock passage the IMF is weakly southward, but immediately after the

Plate 2. Polar projection of the FAST magnetic field perturbations. The data shown in panel c were acquired shortly after the Sudden Impulse (23:45 UT). For these data the polar cap boundary is inferred from keV electron observations.

Figure 3. Solar wind data for an intense cusp region ion outflow event. The data have been lagged by 25 minutes. This lag-time is determined by the time of the Sudden Impulse observed within the magnetosphere. Similar in format to Figure 2.

shock passage the IMF is predominantly in the +y direction. At the tail end of the CME the IMF is strongly southward, and remains so for the rest of the interval.

The FAST data in Plate 2 are similar in format to Plate 1, except that we have used keV electron data to determine the polar cap boundary. The FAST orbit has also evolved, lying in the noon-midnight meridian with the apogee (~4000 km) occurring near the middle of each pass. The data show many of the signatures we might expect on consideration of the forces applied at the magnetopause. For the first interval strong cusp currents are observed, with the delta-B pointing mainly in the +y direction, consistent with the IMF. The field lines in the polar cap are being pulled tailward, which is consistent with the weakly southward IMF at this time. In Plate 2b the cusp stresses are somewhat reduced, but after the shock passage (Plate 2c), the stresses are again large. The net change in the field is of the order 1000 nT on passing through the cusp current in Plate 2c. Taking into account the mapping along field lines, this gives an ionospheric signature about a factor of four larger than discussed in section 2. Given the increase in solar wind velocity and magnetic field strength after the shock passage, this increase is reasonable. Furthermore, the field perturbations are qualitatively similar in Plates 2b and 2c. We would therefore argue that the ion outflow reported by

Moore et al. [1999] arises from enhanced dissipation associated with the increase in applied stress after the shock passage.

The last panel in Plate 2 shows data acquired at the end of the CME, where the IMF is strongly southward. The dominant signature is clearly a sunward field perturbation, consistent with field lines being dragged tailward, and the polar cap is much larger than on the previous orbit. There is an indication of cusp currents, but in this case the deflection of the field is towards dawn, which is consistent with the negative IMF B_y observed at this time.

5. CONCLUSIONS

The major strength of FAST is the extensive suite of high resolution data, both particles and fields, which are being used to understand many of the processes occurring within the auroral acceleration region. The rapid precession in local time of the orbit (~ 3 hours per month) allows measurements to be acquired over the entire auroral oval, further enhancing the ability of FAST to investigate auroral processes. In this paper, however, we have concentrated on the FAST magnetometer observations to emphasize the usefulness of considering the stresses applied to the auroral ionosphere and polar cap. To do this we have used the deviations of the observed field from the model field, rather than converting the magnetometer data to an equivalent current density by taking the derivative of the transverse components along the spacecraft trajectory. This allows us to discuss the data in terms of the high altitude flows and the resultant stresses applied to the ionosphere, as shown schematically in Figure 1.

This "B, v" framework does allow us to place the overall magnetic field signatures in context. In doing so, however, we have neglected effects such as the finite time for information to travel from the magnetosphere and magnetopause to the ionosphere. We have acknowledged the effects of parallel electric fields, in terms of ionospheric slippage, but we have only discussed qualitatively how parallel electric fields could arise. Last, we have neglected neutral winds. Clearly, many auroral and polar cap phenomena are related to information travel times and parallel electric fields, as well as such effects as the neutral wind flywheel. The usefulness of cartoons such as Figure 1 is in specifying the idealized equilibrium. Much of the physics of the auroral zone and polar cap could then be understood in terms of the exchange of energy and momentum between magnetosphere and ionosphere that occurs in trying to achieve this equilibrium.

The two intervals we have shown here demonstrate the clear correlation of the "delta-B's" observed on FAST with variations in the IMF. In many ways this complements the work of *Iijima and Potemra* [1982], who investigated the dependence of region-1 current strength on IMF param-

eters. As they noted, their results implied that reconnection was a major source of these currents. We would agree with that conclusion, but take it one step further. Reconnection may be a significant generator for region-1 currents, but the currents ultimately flow because of the need to accelerate the ionosphere against the drag caused by collisions with the neutral gas.

As a closing comment, taking Figure 1 and applying it the nightside auroral zone may have implications for the flow braking discussed by *Shiokawa et al.* [1998]. Figure 1 implies that the ionosphere will also act to brake any flows imposed by strong earthward streaming in the equatorial magnetosphere, and the equatorial current implied by Figure 1 is in the direction of the inertial current discussed by Shiokawa et al. Clearly this requires further analysis, but we might speculate that the strong braking and enhanced field-aligned currents occur when the flow has extended sufficiently close to the earth that there is rapid communication between the magnetosphere and ionosphere. Consideration of the fundamental frequency for standing Alfvén waves indicates this may the case. *Cummings et al.* [1969] show that at L = 6.6 the fundamental toroidal mode frequency is $\approx$ 60 s for an equatorial density of 1 cm^{-3}. It is therefore possible that ionospheric drag acts as a brake on the flow in addition to field and plasma pressure gradients in the inner magnetosphere. As figure 1 shows, field-aligned currents are a natural consequence of the braking caused by ionospheric drag.

REFERENCES

Armstrong, J. C., and A. J. Zmuda, Triaxial magnetic measurements of field-aligned currents at 800 km in the auroral region: Initial results, *J. Geophys. Res.*, *78*, 6802–6807, 1973.

Coroniti, F. V., and C. F. Kennel, Can the ionosphere regulate magnetospheric convection?, *J. Geophys. Res.*, *78*, 2837–2851, 1973.

Cowley, S. W. H., Magnetospheric asymmetries associated with the Y-component of the IMF, *Planet. Space Sci.*, *29*, 79–96, 1981.

Cummings, W. D., and A. J. Dessler, Field-aligned currents in the magnetosphere, *J. Geophys. Res.*, *72*, 1007–1013, 1967.

Cummings, W. D., R. J. O'Sullivan, and P. J. Coleman, Jr., Standing Alfvén waves in the magnetosphere, J. Geophys. Res., 74, 778–793, 1969.

Deng, W., T. L. Killeen, A. G. Burns, and R. G. Roble, The flywheel effect: ionospheric currents after a geomagnetic storm, *Geophys. Res. Lett.*, *18*, 1845–1848, 1991.

Elphic, R. C., J. Bonnell, R. J. Strangeway, C. W. Carlson, M. Temerin, J. P. McFadden, R. E. Ergun, and W. Peria, FAST

observations of upward accelerated electron beams and the downward field-aligned current region, this issue.

Iijima, T., and T. A. Potemra, The amplitude distribution of field-aligned currents at northern high latitudes observed by Triad, *J. Geophys. Res.*, *81*, 2165–2174, 1976.

Iijima, T., and T. A. Potemra, The relationship between interplanetary quantities and Birkeland current densities, *Geophys. Res. Lett., 9*, 442–445, 1982.

Kelley, M. C., *The earth's ionosphere: plasma physics and electrodynamics*, Academic Press, San Diego, 1989.

Knight, S., Parallel electric fields, *Planet. Space Sci.*, *21*, 741–750, 1973.

Moore, T. E., W. K. Peterson, C. T. Russell, M. O. Chandler, M. R. Collier, H. L. Collin, P. D. Craven, R. Fitzenreiter, B. L. Giles, and C. J. Pollock, Ionospheric mass ejection in response to a coronal mass ejection, *Geophys. Res. Lett.*, *26*, 2339–2342, 1999.

Newell, P. T., C.-I. Meng, and K. M. Lyons, Suppression of discrete aurorae by sunlight, *Nature*, *381*, 766–767, 1996.

Parker, E. N., The alternative paradigm for magnetospheric physics, *J. Geophys. Res.*, *101*, 10,587–10,625, 1996.

Shiokawa, K., W. Baumjohann, G. Haerendel, G. Paschmann, J. F. Fennell, E. Friis-Christensen, H. Lühr, G. D. Reeves, C. T. Russell, P. R. Sutcliffe, and K. Takahashi, High-speed ion flow, substorm current wedge, and multiple Pi 2 pulsations, *J. Geophys. Res.*, *103*, 4491–4507, 1998.

Sugiura, M., and T. A. Potemra, Net field-aligned currents observed by Triad, *J. Geophys. Res.*, *81*, 2155–2164, 1976.

Wright, A. N., Transfer of magnetosheath momentum and energy to the ionosphere along open field lines, *J. Geophys. Res.*, *101*, 13,169–13,178, 1996.

Zmuda, A. J., and J. C. Armstrong, The diurnal variation of the region with vector magnetic field changes associated with field-aligned currents, *J. Geophys. Res.*, *79*, 2501–2502, 1974a.

Zmuda, A. J., and J. C. Armstrong, The diurnal flow pattern of field-aligned currents, *J. Geophys. Res.*, *79*, 4611–4619, 1974b.

Zmuda, A. J., J. H. Martin, and F. T. Heuring, Transverse magnetic disturbances at 1100 kilometers in the auroral region, *J. Geophys. Res.*, *71*, 5033–5045, 1966.

―――――――

C. W. Carlson, Space Sciences Laboratory, University of California at Berkeley, Berkeley, CA 94720

R. C. Elphic, NIS-1, Space and Atmospheric Sciences, Los Alamos National Laboratory, Los Alamos, NM 87545

W. J. Peria, Space Sciences Laboratory, University of California at Berkeley, Berkeley, CA 94720

R. J. Strangeway, Institute of Geophysics and Planetary Physics, University of California at Los Angeles, Los Angeles, CA 90095